

PAPER View Article Online View Journal | View Issue



Cite this: RSC Adv., 2019, 9, 39589

Seunghun Jang,‡^a June Kyu Park,‡^a Minseuk Kim,^b Kee-Sun Sohn, ^b Chang Hae Kim*^a and Hyunju Chang ^b*

0, 1, 2, 3): DFT predictions and synthesis†

Finding new phosphors through an efficient method is important in terms of saving time and cost related to the development of phosphor materials. The ability to identify new phosphors through preliminary simulations by calculations prior to the actual synthesis of the materials can maximize the efficiency of novel phosphor development. In this paper, we demonstrate the use of density functional theory (DFT) calculations to guide the development of a new red phosphor. We performed first-principles calculations based on DFT for pristine and Mn-doped Rb_xK $_{3-x}$ SiF $_7$ (x=0,1,2,3) and predicted their stability, electronic structure, and luminescence properties. On the basis of the results, we then synthesized the stable Rb₂KSiF $_7$:Mn⁴⁺ red conversion phosphor and investigated its luminescence, structure, and stability. As a result, we confirmed that Rb₂KSiF $_7$:Mn⁴⁺ emitted red light with a longer wavelength than that emitted by K₃SiF $_7$:Mn⁴⁺ and a wavelength similar to that of K₂SiF $_6$:Mn⁴⁺. These results show that DFT calculations can provide rational insights into the design of a phosphor material before it is synthesized, thereby reducing the time and cost required to develop new red conversion phosphors.

New red-emitting phosphor $Rb_xK_{3-x}SiF_7:Mn^{4+}$ (x =

Received 31st July 2019 Accepted 19th November 2019

DOI: 10.1039/c9ra05929f

rsc.li/rsc-advances

1. Introduction

White-light-emitting diodes (WLEDs), which have been highlighted as next-generation light sources, have been widely studied because of their outstanding features, which include high durability, high energy conversion efficiency, low power consumption, and environmental friendliness. 1-3 To obtain white light, the strong blue-light emission from an InGaN lightemitting diode (LED) chip must be converted by colorconversion phosphor materials. Among numerous available conversion phosphors, an excellent red phosphor that exhibits a good color-rendering index is needed for WLEDs. Conventionally, CaAlSiN₃:Eu²⁺ (CASN:Eu²⁺) and K₂SiF₆:Mn⁴⁺ are the representative red conversion phosphors with superior performance.4-7 Because of their extensive color gamut and better color-rendering index, these phosphors have been widely used. In addition, a novel red narrow-band phosphor, K₃SiF₇:Mn⁴⁺, with fluorescence characteristics similar to those of the

To address this problem, we considered substituting the K⁺ ions in K₃SiF₇:Mn⁴⁺ with Rb⁺ ions. When Rb⁺, which is a member of the same periodic group as K⁺ but has a larger atomic radius, is substituted for K⁺ in the K₃SiF₇:Mn⁴⁺ system, expansion of the lattice is expected. Such a change in the lattice is reasonably presumed to affect the luminescent properties of the system.

Meanwhile, theoretical approaches for the design of new phosphors can offer more effective ways to explore new conversion phosphor materials.^{5,9} In our previous work, on the basis of first-principles studies based on density functional theory (DFT), we proposed that Sn- or Bi-doped CASN would be an effective alternative to Eu-doped CASN phosphors. Following our theoretical study, Sn- and Bi-doped CASN red phosphors were successfully prepared and their phosphor properties were experimentally demonstrated.^{5,10}

In the present work, we performed first-principles calculations based on DFT for pristine and Mn-doped $Rb_xK_{3-x}SiF_7$ (x=0,1,2,3) and predicted their stability, electronic structure, and luminescence properties. In addition, on the basis of the knowledge gained from first-principles calculations, we synthesized $Rb_2KSiF_7:Mn^{4+}$ as a stable red conversion phosphor

 $K_2SiF_6:Mn^{4+}$ phosphor has recently been introduced.⁸ Although some progress has been made in terms of enhancing the feasibility of its synthesis and improving its decay time, the $K_3SiF_7:Mn^{4+}$ phosphor has a shortcoming in that the wavelength of its main photoluminescence (PL) peak is shorter than that of $K_2SiF_6:Mn^{4+}$, which inhibits its color-rendering index or reduces its color gamut.

[&]quot;Korea Research Institute of Chemical Technology, 141 Gajeong-ro, Yuseong-gu, Daejeon 34114, Republic of Korea

^bFaculty of Nanotechnology and Advanced Materials Engineering, Sejong University, Seoul 05006, Republic of Korea. E-mail: changhae@krict.re.kr; hjchang@krict.re.kr; Fax: +82 42 860 7508; Tel: +82 42 860 7364

 $[\]dagger$ Electronic supplementary information (ESI) available: Atomic geometries for RbK_2SiF_7 and Rb_2KSiF_7, band structures and density of states (DOS) for Rb_xK_3_xSiF_7 structures, atomic and orbital projected DOSs of Rb_3SiF_7, atomic projected DOS on the ground and excited states of Rb_xK_3_xSiF_7:Mn^4+ structures. See DOI: 10.1039/c9ra05929f

 $[\]ddagger$ S. J. and J. K. P. contributed equally to this work.

and verified its PL properties, structure, and stability. The Rb₂KSiF₇:Mn⁴⁺ emitted red light with a wavelength longer than that of the red light emitted by K₃SiF₇:Mn⁴⁺ and similar to that of the light emitted by K2SiF6:Mn4+. These results also show good agreement with the theoretical calculation results that indicated that the simulated emission wavelength of Rb2-KSiF₇:Mn⁴⁺ is the longest among the investigated phosphors. These results demonstrate that DFT calculations can provide rational insights into the properties of a phosphor material before it is synthesized, thereby reducing the time required to develop new red conversion phosphors.

Computational and experimental details

2.1. DFT calculations

The atomic and electronic structures of the $Rb_xK_{3-x}SiF_7$ (x = 0, 1, 2, 3) host materials were examined using the Vienna ab initio simulation package (VASP).11,12 The exchange-correlation functional was approximated using the Perdew-Burke-Ernzerhof (PBE) expression.¹³ The electron-ion interactions were modeled using the projector-augmented wave (PAW) method.14 The electronic wave functions were expanded in a basis set of plane waves using a kinetic energy cutoff of 500 eV. Geometry relaxation steps were performed under the criterion that ionic forces were reduced to less than 0.01 eV \mathring{A}^{-1} .

Mn-doped Rb_xK_{3-x}SiF₇ systems with Mn atoms substituted at Si sites were analyzed using a $1 \times 1 \times 2$ supercell structure. To optimize the geometry of each modeled structure, the kspace integration steps for pristine and Mn-doped Rb_rK_{3-r}SiF₇ structures were performed with finite sampling of the k-points on $7 \times 7 \times 9$ and $7 \times 7 \times 5$ meshes in the Brillouin zone, respectively. For the calculations of electronic structures, such as density of states (DOS) and band-structure calculations, the k-space integration steps for the pure and Mn-doped Rb_xK_{3-x}-SiF₇ structures were performed with finite sampling of the kpoints on $9 \times 9 \times 11$ and $9 \times 9 \times 7$ meshes in the Brillouin zone, respectively.

2.2. Synthesis

The novel red phosphor Rb₂KSiF₇:Mn⁴⁺ was successfully synthesized at room temperature via a two-step procedure, as shown in Fig. 1(a) and (b). Step 1 is the preparation of Rb₂-SiF₆:Mn⁴⁺; step 2 is sintering and washing to obtain the novel red phosphor Rb₂KSiF₇:Mn⁴⁺.

A schematic of the liquid-state reaction (LSR) method is shown in Fig. 1(a). The raw materials used in the synthesis were Rb₂SiF₆ (Fluka, 99.0%), KF (Acros, 99%), KMnO₄ (Junsei Chemical Co., Ltd., 99.3%), KHF₂ (Sigma-Aldrich, 99%), HF (Avantor, 48%), H₂SiF₆ (SAMCHUN, 40%), and H₂O₂ (SAM-CHUN, 34.5%). All chemical reagents were used as obtained without further purification. The overall synthesis process was conducted in a safe environment.

2.2.1. Procedure for synthesizing Mn⁴⁺-activator, K₂MnF₆ (step 1 in Fig. 1). First, we synthesized Mn⁴⁺-activator, K₂MnF₆ according to the following chemical reaction:

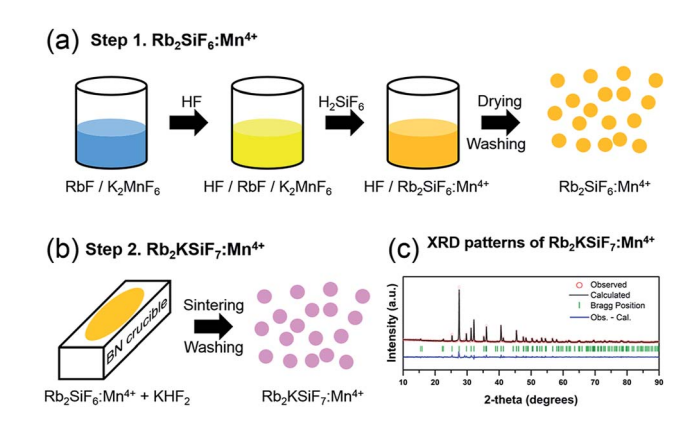


Fig. 1 Overall experimental procedure for the synthesis of the novel red phosphor Rb₂KSiF₇:Mn⁴⁺: (a) procedure for the synthesis of Rb₂-SiF₆:Mn⁴⁺ and (b) procedure for conversion from Rb₂SiF₆:Mn⁴⁺ to Rb₂KSiF₇:Mn⁴⁺. (c) XRD pattern of the Rb₂KSiF₇:Mn⁴⁺ with its corresponding Rietveld refinement (solid line) and residual (observedcalculated)

$$2KMnO_4(s) + 2KF(s) + 10HF(aq) + 3H_2O_2$$

 $\rightarrow 2K_2MnF_6(s) + 8H_2O(1) + 3O_2(g)$

KF and KMnO₄ powders were weighed in the appropriate quantitative stoichiometric ratio using a balance. The weighed powders were placed in a Teflon beaker, and the HF was added. The resultant mixture was stirred for approximately 1 h until the powders had completely dissolved. The color of the mixed solution immediately turned purple upon addition of the HF. H₂O₂ solution was then added dropwise to the reaction solution, which induced precipitation. The precipitated powder was then collected by filtration through filter paper. The obtained solid was dried in an oven for a specific time, resulting in K2MnF6 powder as an intermediate product.

2.2.2. Procedure for synthesizing Rb₂SiF₆:Mn⁴⁺ (step 1 in Fig. 1). Weighed powders of KF and K₂MnF₆ were placed in a Teflon beaker, and HF was added; the resultant mixture was stirred for several hours. The powder dissolved immediately and turned orange. A certain amount of H₂SiF₆ solution was added using a metering pump. The solution was stirred for few additional minutes, and an orange precipitate (Rb₂SiF₆:Mn⁴⁺) formed. The phosphor was collected and washed with acetone several times to remove residues and then dried for several hours in an oven at 110 °C.

2.2.3. Procedure for conversion from Rb₂SiF₆:Mn⁴⁺ to Rb₂KSiF₇:Mn⁴⁺ (step 2 in Fig. 1). Rb₂KSiF₇:Mn⁴⁺ was synthesized via a solid-state reaction method. The prepared Rb₂SiF₆:-Mn⁴⁺ phosphor and various ratios of KHF₂ were mixed an agate mortar until a homogeneous mixture was obtained. The mixed powder was sintered in a BN crucible at 300 °C for several hours under N2/H2 mixture gas (N2 gas: 100-75%, H2 gas: 0-25%, flow rate: $600 \text{ cm}^3 \text{ min}^{-1}$) in a horizontal tube furnace. The products were cooled to room temperature, ground, and then washed with ethanol several times to remove the remaining substances and to prevent aggregation.

(a) RbK₂SiF₇ Rb₂KSiF₇ Rb₃SiF₇ Formation Energy (eV/atom) -3.05 -3.10

Fig. 2 (a) Atomic geometries of $Rb_xK_{3-x}SiF_7$. The violet, pink, blue, and white balls represent K, Rb, Si, and F atoms, respectively. (b) Bulk formation energies of the $Rb_xK_{3-x}SiF_7$ structures.

Rb SiF

RbK,SiF

2.3. Characterization

Paper

The crystal structures of the phosphors (Rb₂KSiF₇:Mn⁴⁺) were determined by X-ray diffraction (XRD, Rigaku D/Max 220V) using Cu K_{\alpha} radiation (Ni filter, voltage: 40 kV, current: 40 mA), as shown in Fig. 1(c). To investigate the morphology and the size of the prepared phosphors, we used scanning electron microscopy (SEM; JEOL JSM-6360). The composition of the samples was analyzed by energy-dispersive X-ray spectrometry (EDS) using a spectrometer (Bruker Quantax 200) with an energy resolution <127 eV (HV: 20.0 kV). The optical characteristics of the phosphors were examined at room temperature using a photoluminescence spectrometer (DARSA PRO-5000) and a Xe light source (500 W). Thermogravimetric analysis (TGA) and differential thermal analysis (DTA) of the phosphors were conducted on a Thermo Plus EVO II (TG8120 series, DSC 8230) at a heating rate of 5 °C min⁻¹ under flowing N₂ gas.

3. Results and discussion

Fig. 2(a) shows the atomic geometries of the $Rb_xK_{3-x}SiF_7$ structures. With increasing x in $Rb_xK_{3-x}SiF_7$, the lattice parameters and cell volume increase, as shown in Table 1, because the atomic radius of Rb (2.35 Å) is slightly larger than that of K (2.20 Å).¹⁵ The trend of the calculated lattice parameters with increasing Rb content is consistent with the trend of

Table 1 Experimental and theoretical lattice parameters for Rb_xK_{3-x}SiF₇

| Tetragonal (P4/mbm) | Experiment | | | Theory (this work) | | |
|---|--------------|--------------|--------------|----------------------|----------------------|----------------------|
| | a (Å) | b (Å) | c (Å) | a (Å) | b (Å) | c (Å) |
| K ₃ SiF ₇ RbK ₂ SiF ₇ Rb ₂ KSiF ₇ | 7.74 7.88 | 7.74 7.88 | 5.56 5.72 | 7.87 7.94 8.04 | 7.87 7.94 8.04 | 5.64 5.72 5.82 |
| Rb ₃ SiF ₇ | 7.95 | 7.95 | 5.82 | 8.14 | 8.14 | 5.92 |

the experimental lattice parameters. 16,17 In particular, in the cases of binary cations (Rb⁺ and K⁺), various structural configurations in which Rb⁺ or K⁺ ions occupy positions in the unit cell are possible (see Fig. S1 in ESI†). The RbK2SiF7 and Rb2-KSiF₇ atomic geometries shown in Fig. 2(a) were chosen as the structures with the most stable total energy among the various investigated configurations. These two energetically preferred structures exhibit interesting structural features. The RbK₂SiF₇ and Rb₂KSiF₇ atomic geometries include K-2D-layer (green trapezium) and K-1D-chain (red arrow) substructures within their atomic structures, respectively (see Fig. S2 in ESI†). We speculated that such substructures energetically stabilize their associated atomic structures.

In addition, we calculated the bulk formation energies of the $Rb_xK_{3-x}SiF_7$ structures. The formation energy, ΔH_f , for Rb_x - $K_{3-x}SiF_7$ is given by $\Delta H_f = E_{tot} - \sum \mu_i x_i$, where E_{tot} is the total

energy of the structure, μ_i is the chemical potential of element i, and x_i is the number of elements i in the structure. ¹⁸ In terms of the design of a new host material for conversion phosphors, the DFT formation energy can be an important indicator for determining whether a phosphor material can be synthesized. As shown in Fig. 2(b), all of the $Rb_xK_{3-x}SiF_7$ structures have negative formation energies, which indicates that all of the structures we considered can be synthesized. Among these except Rb₂KSiF₇ have been reported compounds, all experimentally.16,17

Furthermore, we calculated the energy band structures and DOSs of the $Rb_xK_{3-x}SiF_7$ system (see Fig. S3 in ESI†). With increasing Rb content, the bandgap of the host material system decreases from 5.59 eV to 5.33 eV. This decrease of the bandgap energy is related to the increase of the lattice parameters with increasing Rb content. Because of the large radius of Rb atoms, an increase of the Rb content (with Rb substitution at the K sites) leads to an expansion of the $Rb_xK_{3-x}SiF_7$ unit-cell volume. Accordingly, the increase of the cell volume leads to weakening of the binding forces of the atoms' valence electrons. Consequently, the valence electrons become freer with increasing interatomic distance, which eventually reduces the bandgap which corresponds to the energy required for valence electrons to be promoted to the conduction band (CB).

From the atomic projected DOSs, we find that, although the CB is derived mainly from the Rb d state, the F p state contributes to the upper valence band (VB) (see Fig. S4 in ESI†). An enlarged image of the CB region from 5 eV to 10 eV is shown in the inset of each DOS diagram. As the Rb content increases, the Rb d state (in the CB) and Rb p state (near -8 eV, marked with a blue star) are enhanced. These Rb-related DOSs do not appear to strongly affect the F- or Si-related states.

One of the important factors in the development of conversion red phosphors is their emission wavelength. If the emission wavelength of the candidate material can be predicted before the material is actually synthesized, the phosphor development time would be dramatically reduced, leading to the efficient design of effective phosphor materials. Consequently, the ability to predict the emission energy of the doping system is important. For Mn-doped phosphor systems, the

emission light is known to originate from the spin-flip transition of Mn⁴⁺, such as the transition from the ²E_g excited state to the ${}^{4}A_{2g}$ ground state. As shown in Fig. 3(a), low-spin (1 μ_{B}) and high-spin (3 $\mu_{\rm B}$) states correspond to the $^2{\rm E_g}$ excited state and the ⁴A_{2g} ground state, respectively. ¹⁹ Therefore, the emission energy of Mn⁴⁺ can be predicted by calculating the total energy difference between the low-spin state and the high-spin state. The emission energy was calculated according to the equation Emission Energy = $E_{\text{low-spin}}$ - $E_{\text{high-spin}}$, where $E_{\text{low-spin}}$ and $E_{\text{high-spin}}$ are the total energies of Mn⁴⁺ doped systems with relaxed low-spin (1 μ_B) and high-spin (3 μ_B) states, respectively.

To calculate emission energies that account for the effects of Mn doping on the four $Rb_xK_{3-x}SiF_7$ (x = 0, 1, 2, 3) host materials, we first calculated the atomic and electronic structures of Mn-doped $Rb_xK_{3-x}SiF_7$. Fig. 3(b) shows the atomic geometry of the Rb₂KSi_{0.75}Mn_{0.25}F₇ structure. To minimize the effect of Mn-Mn interaction on the electronic structure, we introduced a 1 \times 1×2 super cell structure. Among four Si sites (Si₁, Si₂, Si₃, and Si₄ sites), a Si atom was replaced with a Mn atom and the minimum Mn-Mn interatomic distance was 7.8 Å. Fig. S5 in ESI† shows the atomic projected DOSs on the ⁴A_{2g} ground (left side) and ²E_g excited (right side) states of the Rb_xK_{3-x}SiF₇:Mn⁴⁺ structures. In all of the DOSs, both the $t_{\rm 2g}$ and $e_{\rm g}$ states of Mn atoms are hybridized with the F p states. That is, the t_{2g} and e_{g} states between the bandgap of the host are donated by the Mn

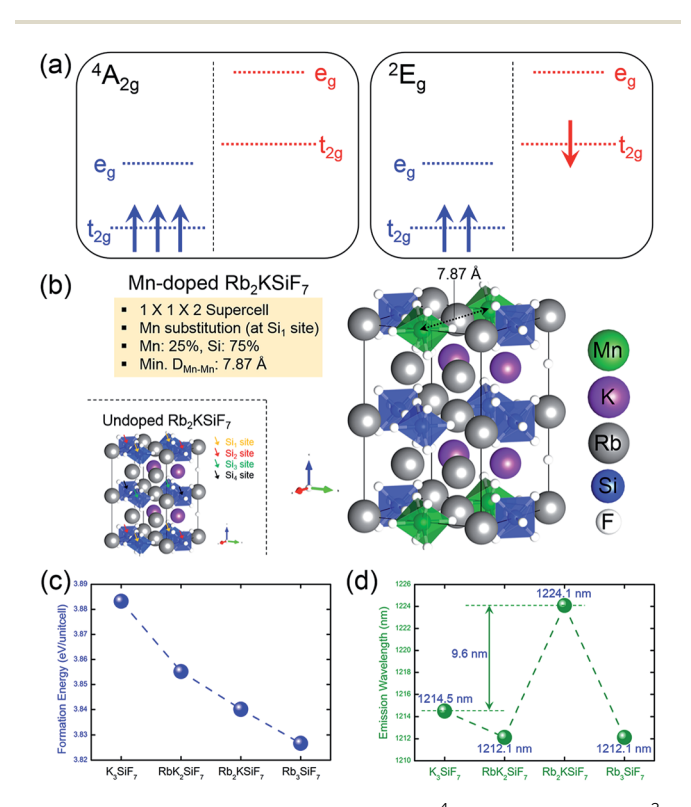


Fig. 3 (a) Schematic energy diagrams of the ${}^4A_{2g}$ ground state and ${}^2E_{g}$ excited state of Mn⁴⁺. (b) Atomic geometries of Rb₂KSiF₇ (undoped) and Rb₂KSi_{0.75}Mn_{0.25}F₇ (Mn-doped) structures. The green, violet, pink, blue, and white balls represent Mn, K, Rb, Si, and F atoms, respectively. (c) Formation energies of $Rb_xK_{3-x}SiF_7:Mn^{4+}$ with Mn substituted at Sisites and (d) the simulated emission wavelengths of the Mnsubstituted products

3d and the F 2p orbitals. In addition, the ${}^4A_{2g}$ ground and 2E_g excited states have high-spin (3 μ_B) and low-spin (1 μ_B) configurations, respectively. In particular, in the ²E_g excited state, a small Jahn-Teller distortion will eventually manifest as splitting of the t_{2g} and e_g states, as shown in the right side of Fig. S5 in ESI†.19 These DOS results are similar to those reported in a previous study.19 No particular trend of the mid-gap states (t2g and e_{α} states) with respect to the Rb content was found.

From the total energies of the ground states, we also calculated the formation energies for substitution of Mn at the Si site in $Rb_xK_{3-x}SiF_7$. The formation energy for Mn substitution, $E_{\text{Mn-sub}}^{\text{form}}$, was calculated to assess the ease with which a Mn atom can replace a Si atom in a certain host material. It was calculated according to the equation $E_{
m Mn-sub}^{
m form} =$ $E_{\text{Mn:RKSF}} + \mu_{\text{Si}} - (E_{\text{RKSF}} + \mu_{\text{Mn}})$, where $E_{\text{Mn:RKSF}}$ is the total energy of the ground state of $Rb_xK_{3-x}SiF_7:Mn^{4+}$, E_{RKSF} is the total energy of undoped $Rb_xK_{3-x}SiF_7$, μ_{Si} is the total energy per atom of bulk Si, and μ_{Mn} is the total energy per atom of bulk Mn. As shown in Fig. 3(c), as the Rb content increases, the formation energy for Mn substitution decreases. This trend is attributed to the lattice expansion induced by the Rb substitution promoting Mn doping (at Si sites).

The results in Fig. 3(d) confirm that the simulated emission energy value fluctuates irrespective of the Rb content. Notably, the Rb₂KSiF₇:Mn⁴⁺ exhibits the longest simulated emission wavelength among the Rb_xK_{3-x}SiF₇:Mn⁴⁺ phosphors. On the basis of this result, we expected the light emission from Rb2-KSiF₇:Mn⁴⁺ to shift toward longer emission wavelengths compared with the wavelengths of the emissions from K₃SiF₇:Mn⁴⁺. In terms of material design of a new conversion phosphor, the aforementioned results provide an important guideline for the synthesis of host materials.

On the basis of the material insights gained thus far through theoretical investigations, we attempted to synthesize a new red conversion phosphor corresponding to Mn-doped Rb_xK_{3-x}SiF₇ (x > 1) using various methods. As a result, we obtained three phosphors: K₃SiF₇:Mn⁴⁺, Rb₃SiF₇:Mn⁴⁺ and Rb₂KSiF₇:Mn⁴⁺. The K₃SiF₇:Mn⁴⁺ phosphor has already been reported.⁸ Thus, we successfully synthesized two new conversion red phosphors, Rb₃SiF₇:Mn⁴⁺ and Rb₂KSiF₇:Mn⁴⁺, with a host material containing Rb. For reference, RbK₂SiF₇:Mn⁴⁺, which has not been reported in the ICSD database, was also not obtained in the present study. In addition, Rb₃SiF₇:Mn⁴⁺, which we successfully synthesized, was very unstable, exhibiting sensitivity to moisture; it structure fragmented soon after it was synthesized. However, the Rb₂KSiF₇:Mn⁴⁺ red phosphor exhibited very stable structural characteristics.

The procedure for the synthesis of Rb₂KSiF₇:Mn⁴⁺ is detailed in Fig. 1(a) and (b) and in Section 2.2. The crystallographic data (see Table S1 in ESI†) determined from Rietveld refinement with XRD patterns of the synthesized Rb₂KSiF₇:Mn⁴⁺, as the first conclusive evidence of the successful synthesis of Rb2KSiF7:-Mn⁴⁺, shows good agreement with the reported experimental lattice parameters for Rb₂KSiF₇ in Table 1.^{16,17}

Fig. 4(a) shows the normalized PL ($\lambda_{ex} = 460$ nm) and photoluminescence excitation (PLE) ($\lambda_{em} = 630 \text{ nm}$) spectra of the K₂SiF₆:Mn⁴⁺, K₃SiF₇:Mn⁴⁺ and Rb₂KSiF₇:Mn⁴⁺ phosphors.

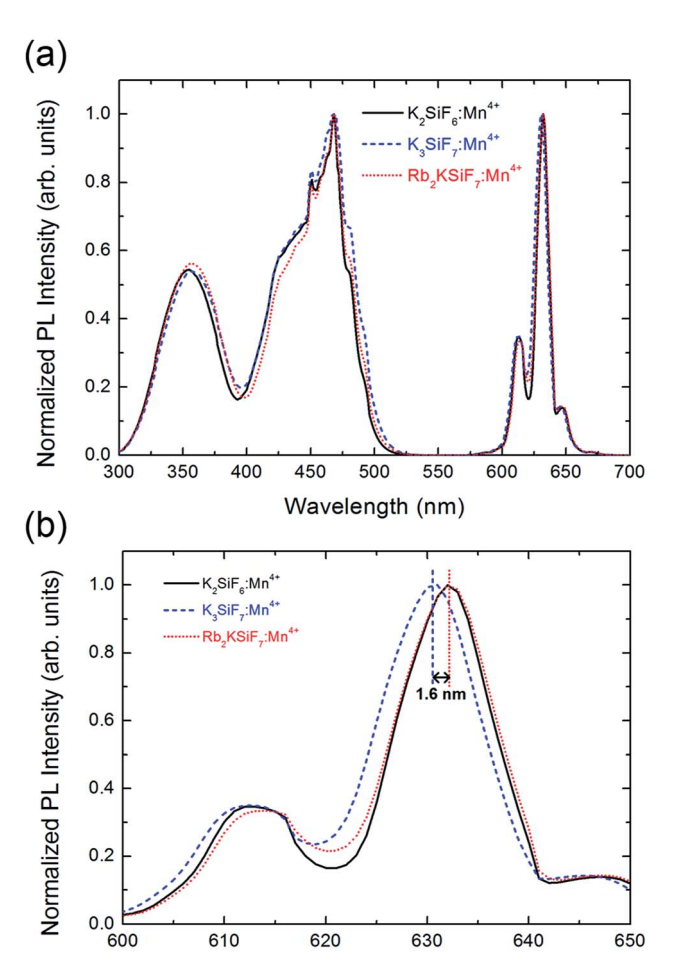


Fig. 4 (a) Normalized PL ($\lambda_{ex}=460$ nm) and PLE ($\lambda_{em}=630$ nm) spectra of K₂SiF₆:Mn⁴⁺, K₃SiF₇:Mn⁴⁺, and Rb₂KSiF₇:Mn⁴⁺ phosphors. (b) An enlargement of the PL spectra in the wavelength range from 600 nm to 650 nm.

Wavelength (nm)

As shown in the right side of the Fig. 4(a), all three phosphors not only show very strong and narrow red luminescence in the wavelength region near 630 nm but also show very stable excitation from 330 nm to 480 nm. To examine the PL results more closely, the spectral region from 600 nm to 650 nm was enlarged (Fig. 4(b)). Here, Rb₂KSiF₇:Mn⁴⁺ clearly emits longerwavelength light than K₃SiF₇:Mn⁴⁺ and has an emission wavelength almost equal to that of K₂SiF₆:Mn⁴⁺. Furthermore, the PL efficiency of Rb₂KSiF₇:Mn⁴⁺ sample (having the highest PL) corresponds to 85% of that of K₂SiF₆:Mn⁴⁺ (93% of that of K₃SiF₇:Mn⁴⁺), as shown in Fig. S6 in ESI.† These results indicate that luminescence with an emission wavelength similar to that of the conventional K₂SiF₆:Mn⁴⁺ phosphor can be induced from a Rb-containing quaternary fluoride phosphor. It also shows good agreement with the theoretical calculation results indicating that the simulated emission wavelength of Rb2-KSiF7:Mn4+ is the longest among the investigated phosphors (Fig. 3(d)); thus, such calculation results can provide rational insights into the properties of a phosphor material before it is synthesized.

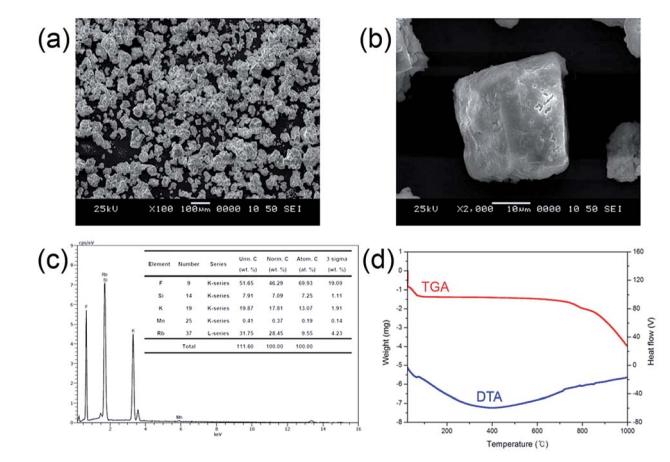


Fig. 5 (a) and (b) SEM images, (c) EDS diagram, and (d) TGA and DTA curves of the $Rb_2KSiF_7:Mn^{4+}$ phosphor.

Particle morphology is a key factor for phosphor materials used in white LEDs. It is influenced by various physicochemical parameters such as sintering temperature, holding time, precursor materials, chemical composition, crystal structure, and homogeneity, especially when the powders are produced by the solution process via amorphous precursor particles. The morphologies of the particles of the synthesized phosphor materials were observed by SEM. Fig. 5(a) and (b) show the morphology of the Mn⁴⁺-doped Rb₂KSiF₇ powder. Particles with various sizes (approximately 50-100 μm) and shape distributions are observed to be dispersed as shown in Fig. 5(a). In assessing the suitability of the red conversion phosphor for use in white LEDs, not only its morphological properties but also its thermal characteristics should be considered. Fig. 5(d) displays the TGA and DTA curves of the Rb₂KSiF₇:Mn⁴⁺ phosphor. The TGA result shows over two the steps weight drops at around 700 °C and 800 °C. Moreover, DTA exhibits two DTA peaks at 710 °C and 790 °C. These results indicate that the Rb₂KSiF₇:Mn⁴⁺ phosphor is not only decomposed over the two steps into SiF4 and alkali metal fluorides (RbF or KF) but also thermally stable to 750 °C.²⁰ Apart from thermal stability of phosphor structure, we checked the temperature-dependent PL properties of Rb₂KSiF₇:Mn⁴⁺ (see Fig. S7 in ESI†). As a results, the luminescent property of Rb₂KSiF₇:Mn⁴⁺ phosphor exhibits thermally stable properties up to 125 °C, but, above 150 °C, PL quenching occurs rapidly. Even if the temperature was lowered again, PL intensity degraded by high temperature was not recovered.

4. Conclusions

We performed first-principles calculations based on DFT for pristine and Mn-doped $Rb_xK_{3-x}SiF_7$ (x=0,1,2,3) and predicted their stability, electronic structure, and luminescence properties. According to the results of calculations for the $Rb_xK_{3-x}SiF_7$ (x=0,1,2,3) host structures performed prior to the calculation for the Mn-doped system, all of the compounds

exhibit a large negative bulk formation energy, which indicates that all of the structures considered in this study could be synthesized. Moreover, as the content of Rb increases in the Rb_rK_{3-r}SiF₇ host system, their bandgap energy decreases from 5.59 eV to 5.33 eV. From the atomic projected DOSs, we found that, while the CB is derived mainly form the Rb d state, the upper VB arises from the F p state. For the Mn-doped Rb_r- $K_{3-r}SiF_7$ phosphor system, we calculated the formation energy for Mn substitution and the simulated emission energy of each structure. As a result, we found that, with increasing Rb content, the formation energy for Mn substitution decreases. This trend was attributed to the Rb substitution expanding the lattice because of larger size of Rb ion than K ion. The lattice expanding could promote Mn doping at Si sites.

On the basis of the knowledge gained through the simulations, we next synthesized red conversion phosphors and investigated their luminescence, structure, and stability. As a result, we successfully prepared the stable new red conversion phosphor Rb₂KSiF₇:Mn⁴⁺. In addition, the Rb₂KSiF₇:Mn⁴⁺ emitted at a longer wavelength than the K3SiF7:Mn4+ and exhibited an emission wavelength similar to that of K₂SiF₆:Mn⁴⁺. This similarity indicated that a red phosphor with a luminescence wavelength similar to that of the conventional K₂SiF₆:Mn⁴⁺ phosphor was prepared as a quaternary fluoride phosphor containing Rb. It also showed good agreement with our theoretical calculation results, which shows that Rb₂-KSiF₇:Mn⁴⁺ exhibited the longest simulated emission wavelength among the four Mn-doped structures.

Collectively, these results demonstrate that DFT calculations can provide rational insights into the properties of a red phosphor material before it is synthesized, thereby reducing the time and cost required to develop new red conversion phosphors.

Conflicts of interest

There are no conflicts to declare.

Acknowledgements

This research was supported by the Nano Material Technology Development Program through the National Research Foundation of Korea funded by the Ministry of Science and ICT (NRF-2016M3A7B4025408).

Notes and references

- 1 Y. H. Kim, P. Arunkumar, B. Y. Kim, S. Unithrattil, E. Kim, S.-H. Moon, J. Y. Hyun, K. H. Kim, D. Lee, J.-S. Lee and W. B. Im, Nature, 2017, 16, 543-550.
- 2 M. Zhao, H. Liao, L. Ning, Q. Zhang, Q. Liu and Z. Xia, Adv. Mater., 2018, 30, 1802489.
- 3 S. Liang, M. Shang, H. Lian, K. Li, Y. Zhang and J. Lin, J. Mater. Chem. C, 2017, 5, 2927-2935.
- 4 X. Piao, K.-I. Machida, T. Horikawa, H. Hanzawa, Y. Shimomura and N. Kijima, Chem. Mater., 2007, 19, 4592-4599.
- 5 S. Jang, J. Im, B. K. Bang, C. H. Kim, H. Chang and K.-J. Kong, RSC Adv., 2015, 5, 39319-39323.
- 6 T. Takahashi and S. Adachi, J. Electrochem. Soc., 2008, 155, E183-E188.
- 7 H. F. Sijbom, R. Verstraete, J. J. Joos, D. Poelman and P. F. Smet, Opt. Mater. Express, 2017, 7, 3332-3365.
- 8 M. Kim, W. B. Park, B. Bang, C. H. Kim and K.-S. Sohn, J. Am. Ceram. Soc., 2017, 100, 1044-1050.
- 9 Y. Zhuo, A. M. Tehrani, A. O. Oliynyk, A. C. Duke and J. Brgoch, Nat. Commun., 2018, 9, 4377.
- 10 C. H. Kim, B. K. Bang, J. K. Park, K.-J. Kong, H. Chang, J. Im, S. Jang and K. S. Choi, KR 101790541, 2017.
- 11 G. Kresse and J. Furthmüller, Phys. Rev. B: Condens. Matter Mater. Phys., 1996, 54, 11169-11186.
- 12 G. Kresse and J. Hafner, Phys. Rev. B: Condens. Matter Mater. Phys., 1993, 47, 558-561.
- 13 J. P. Perdew, K. Burke and M. Ernzerhof, Phys. Rev. Lett., 1996, 77, 3865-3868.
- 14 P. E. Blochl, Phys. Rev. B: Condens. Matter Mater. Phys., 1994, 50, 17953-17979.
- 15 J. C. Slater, J. Chem. Phys., 1964, 41, 3199.
- 16 D. L. Deadmore and W. F. Bradley, Acta Crystallogr., 1962, 15, 186-189.
- 17 B. Hofmann and R. Hoppe, Z. Anorg. Allg. Chem., 1979, 458, 151-162.
- 18 S. Kirklin, J. E Saal, B. Meredig, A. Thompson, J. W. Doak, M. Aykol, S. Rühl and C. Wolverton, npj Comput. Mater., 2015, 1, 15010.
- 19 M. H. Du, J. Mater. Chem. C, 2014, 2, 2475-2481.
- 20 R. Verstraete, H. F. Sijbom, J. J. Joos, K. Korthout, D. Poelman, C. Detavernier and P. F. Smet, ACS Appl. Mater. Interfaces, 2018, 10, 18845-18856.